Nanoscale

ROYAL SOCIETY OF CHEMISTRY

PAPER

View Article Online
View Journal | View Issue

Cite this: *Nanoscale*, 2024, **16**, 3492

Fabrication of highly luminescent and thermally stable composites of sulfur nanodots through surface modification and assembly†

Bingye Sun, Yu-e Shi,* Jiaqi Guo and Zhenguang Wang *

Sulfur nanodots (S-dots) have emerged as a promising luminescent material to excel over traditional heavy metal-based quantum dots. However, their relatively low emission efficiency and poor thermal stability in the solid state have limited their wide applications in photoelectric devices. In this work, highly luminescent, with a photoluminescence quantum yield higher than 50%, and thermally stable composites of S-dots were produced through modulating their surface states and aggregation behaviors by introducing pyromellitic dianhydride (PMDA) and benzoyleneurea (BEU), respectively. PMDA eliminated the relatively short-lived surface states and defects on the surface of S-dots and BEU regulated the aggregation states and facilitated the energy transfer from BEU to S-dots. The as-obtained composites also showed significantly improved thermal stability compared to S-dots, aided by the hydrophobic chemical groups and dense matrix of PMDA and BEU, which extended their applications in fabricating light-emitting diodes. Our presented results provide a new approach to produce highly luminescent S-dots, which widen their applications in the fields of bioimaging, sensing, photoelectric devices, and environmental science.

Received 10th December 2023,
Accepted 29th December 2023

DOI: 10.1039/d3nr06292a

rsc.li/nanoscale

Introduction

Sulfur nanodots (S-dots), a type of newly developed metal-free photoluminescence (PL) nanomaterial, have received intensive research interest because of their low toxicity, tunable PL, abundance of precursors, and anti-fungal properties.[1–6] Tremendous efforts have been devoted to converting bulk sulfur into luminescent nanodots, and they showed great potential for applications in light-emitting diodes (LEDs),[1,7] bioimaging,[8,9] photocatalysis,[10,11] and chemical sensing.[12–14] Shen and co-workers proposed the synthesis of S-dots through etching of bulk elemental sulfur using an alkali with the stabilization of surfactants. S-dots were produced with excitation energy-dependent emissions in the blue-to-green region and a PL quantum yield (QY) of 3.8%.[15] However, their PL efficiency is rather low to fulfil the strict requirements for applications in optoelectronics[16] and nanobiology.[17] We and other groups[12,18–20] have developed hydrogen peroxide and oxygen-assisted strategies to control the size, eliminate surface traps, and fine-tune the emission of S-dots, achieving an improved quantum yield (QY) of higher than 20%. Research efforts also engaged in introducing ultrasonication,[21] microwave,[22] and hydrothermal[23,24] treatments to modulate the size, edge, core, and surface states of S-dots, which significantly promoted the emission efficiency to higher than 80% in colloidal solution.

State Key Laboratory of New Pharmaceutical Preparations and Excipients, Key Laboratory of Analytical Science and Technology of Hebei Province, Key Laboratory of Medicinal Chemistry and Molecular Diagnosis, Ministry of Education, College of Chemistry and Materials Science, Hebei University, Baoding 071002, PR China. E-mail: zgwang@hbu.edu.cn, shiyue1220@163.com

† Electronic supplementary information (ESI) available. See DOI: https://doi.org/10.1039/d3nr06292a

Zhenguang Wang

Zhenguang Wang received his PhD degree in 2017 from City University of Hong Kong. He is now a Professor at the College of Chemistry and Materials Science, Hebei University, China. His research interests include the synthesis of luminescent nanomaterials with a focus on metal nanoclusters and sulfur quantum dots and their applications in optoelectronic devices and chemical sensing.

Benefiting from these research efforts and achievements, S-dots have been tested as phosphors for light-emitting diodes (LEDs). However, compared with their competitors, such as rare-earth element-doped inorganic materials, CdTe and perovskite-based quantum dots,[25–27] they showed a relatively low emission efficiency and poor thermal stability in the solid state. This is caused by a significant decrease in the PL QY after processing the S-dots in colloidal solution to the solid state, together with the relatively low melting point of sulfur-based materials.[28] Some groups engaged in promoting the solid photophysical properties of S-dots by modulating their surface states through producing their composite materials with $BaSO_4$,[29] metal–organic frameworks (MOFs)[30–32] and polymers.[33,34] An improved PL QY was achieved on these composite materials. However, they are still inferior to these competitors. In addition, research on the production of S-dots with excellent thermal stability, in terms of both structure and PL behaviours, is more challenging.

In this work, we solved these issues through modulating the photophysical properties of S-dots by controlling their surface states and aggregation behaviours. The surface S-dots were modulated by modification with pyromellitic dianhydride (PMDA) through covalent bonding, producing a composite of S-dots@PMDA. Benzoyleneurea (BEU) was also used to regulate the aggregation states of S-dots in the solid state by acting as a lube, producing a composite of S-dots@BEU. Both S-dots@PMDA and S-dots@BEU showed an improved PL intensity, attributed to the elimination of the relatively short-lived surface states and defects on the surface of S-dots and the energy transfer from BEU to S-dots, respectively. S-dots@PMDA and S-dots@BEU also showed significantly improved thermal stability compared to S-dots, aided by the hydrophobic chemical groups and dense matrix of PMDA and BEU. These improved photophysical and thermal properties permit the fabrication of S-dot-based LED devices by combining UV LED chips and composites of S-dots and commercial phosphors.

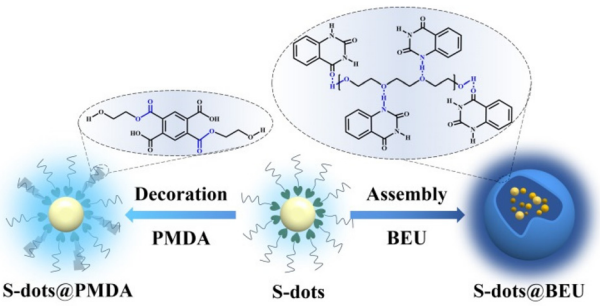

Fig. 1 Schematic illustration of producing S-dots@PMDA and S-dots@BEU through surface modification (left) and assembly (right).

Results and discussion

S-dots were synthesized through a previously reported H_2O_2-assisted top-down method.[18] S-dots were well dispersed in aqueous solution with quasi-spherical in shape and a diameter of 2.4 nm (Fig. S1†). S-dots showed typical excitation-dependent emission in the blue–green region (from 400 to 450 nm), as shown in Fig. S2.† Then, S-dots were processed into composite materials through reacting with pyromellitic dianhydride (PMDA) and benzoyleneurea (BEU), followed by evaporating the excess aqueous solvent to convert them into powder. The as-obtained products were denoted as S-dots@PMDA and S-dots@BEU, respectively. PMDA tended to hydrolyze into pyromellitic acid after absorbing water, which was supposed to react with the hydroxyl groups on the surface of S-dots, forming ester linkages (Fig. 1). In contrast, BEU was rather stable to form chemical bonds with S-dots, which may be used to regulate the aggregation states of S-dots in the solid state by acting as a lube (Fig. 1). As expected, reacting with PMDA resulted in a slightly enlarged size of S-dots (from 2.43 to 3.83 nm), without effecting their dispersion and colloidal stability (Fig. 2a). The HRTEM images show the characterized lattice fringes of S-dots (0.21 nm),[35] suggesting the integrity of the elemental sulfur core in S-dots. In contrast, introducing BEU resulted in the assembly of S-dots into bigger clusters with a size of around 80 nm (Fig. 2b). FTIR spectra were used to study the molecular interactions among S-dots@PMDA and S-dots@BEU. As shown in Fig. 2c, S-dots showed the characteristic FTIR spectral peaks of PEG located at 2870, 943, and 1450 cm^{-1}, corresponding to the stretching vibrations of C–H and O–H and the bending vibration of C–H, respectively.[36,37] After decorating with PMDA, several new bands from 1700 to 1800 cm^{-1} appeared, attributed to the ester absorption formed through the reaction between the –COOH group and the –OH group from PMDA and PEG, respectively.[38] In contrast, no additional or deleted peaks were observed after introducing BEU into S-dots (Fig. 2c). Note that loading BEU resulted in the appearance of slightly broader absorption bands at around 3200 cm^{-1}, suggesting the formation of hydrogen bonds.

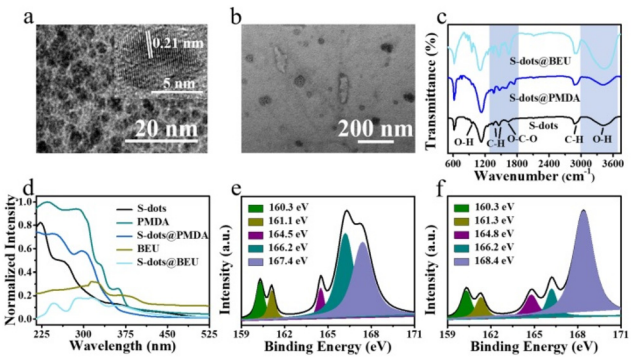

Fig. 2 Characterization of S-dots@PMDA and S-dots@BEU. TEM images of S-dots@PMDA (a) and S-dots@BEU (b). (c) FTIR spectra of S-dots, S-dots@PMDA, and S-dots@BEU, as indicated on the frame. (d) UV-visible absorption spectra of S-dots, S-dots@PMDA, S-dots@BEU, and pure molecules of PMDA and BEU, as indicated on the frame. High-resolution S 1s XPS spectra of S-dots@PMDA (e) and S-dots@BEU (f).

Thus, we concluded that PMDA was linked with S-dots through covalent bonds and S-dots@BEU was cross-linked by hydrogen bonds. This is further confirmed by the results of Raman spectra (Fig. S3†). Processing S-dots into S-dots@PMDA and S-dots@BEU resulted in the emergence of a relative broad peak at around 3000 cm^{-1}, suggesting the presence of hydrogen bonds. S-dots@BEU showed almost identical spectral behavior with that of S-dots, excluding the formation of other covalent bonds. Instead, newly added peaks at 832, 884 and 1444 cm^{-1} were observed in the case of S-dots@PMDA, suggesting the formation of an ester. These observations were also consistent with the results of UV-visible absorption spectral measurements. As shown in Fig. 2d, S-dots showed three absorption bands at 223, 266, and 360 nm, corresponding to the n → σ* transition of elemental sulfur and polysulfides and bandgap transitions of elemental sulfur, respectively.[39] The absorption bands at 332 and 362 nm, assigned to the n → π* transition of C═O and extended π conjugation, of PMDA disappeared, suggesting the reaction of –COOH groups in PMDA@S-dots.[40] The composite materials of S-dots@BEU showed the integrated absorption behavior of S-dots and BEU without newly added or deleted absorption bands (Fig. 2d). The full peaks were fitted in the high resolution S 1s XPS spectra of PMDA@S-dots located at 160.3, 161.1, 164.5, 166.2, and 167.4 eV (Fig. 2e), corresponding to S^{2-}, polysulfide, elemental sulfur, oxidized sulfur composition of SO_3^{2-} ($2p_{3/2}$), SO_3^{2-} ($2p_{1/2}$), respectively.[41] S-dots@BEU showed almost identical spectral behaviors, except that the content of SO_4^{2-} was much higher than that of S-dots@PMDA (Fig. 2f, Table S1†). This can be explained by the fact that these anions were exchanged and released during the surface reaction of PMDA with S-dots.

Interestingly, after processing S-dots into a composite of S-dots@PMDA and S-dots@BEU, 4.8-fold and 36-fold increases were observed in the fluorescence intensities (Fig. 3a). To get the best PL performances, the effects of synthesis conditions, including the reaction amount of PMDA and BEU and reaction pH, on the PL intensities of products were systematically studied. As shown in Fig. S4 and S5,† the highest PL intensities were achieved by introducing 0.08 g of PMDA, reacting at the pH of 10, and adding 5 mg of BEU, reacting at the pH of 11, for producing PMDA@S-dots and S-dots@BEU, respectively. Similar to S-dots, S-dots@PMDA also showed excitation-dependent emission properties, at the excitation wavelength from 310 to 410 nm (Fig. 3b, Fig. S6†). In addition, the composites also showed excitation-dependent PL QYs from 5.9% to 50% at the excitation wavelength from 310 to 400 nm. This suggests that the surface chemical reaction did not lead to the decomposition of S-dots and varying of emission species. Noted that a 10 nm red shift was observed in the peak maximum of the PL excitation spectra (Fig. 3c) and an extension of the emission lifetime from 2.55 ns to 8.06 ns (Fig. 3d, Table S2†) was observed after modifying S-dots with PMDA. This can be attributed to the modulation of the surface states of S-dots by surface treatments. The introduction of PMDA eliminated the relatively short-lived surface states and defects

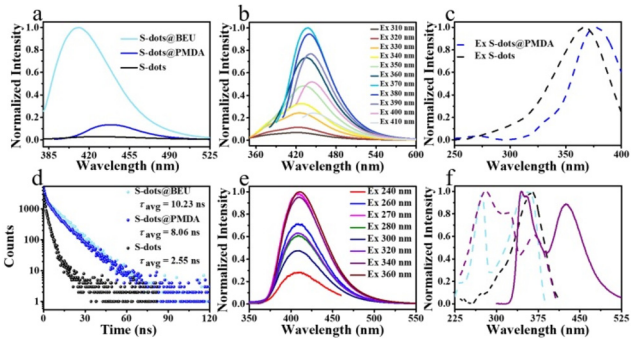

Fig. 3 Photophysical properties of S-dots@PMDA (e) and S-dots@BEU. (a) PL emission spectra of S-dots (black line, excited at 360 nm), S-dots@PMDA (blue line, excited at 370 nm), and S-dots@BEU (cyan line, excited at 360 nm). (b) PL emission spectra of S-dots@PMDA excited at different wavelengths. (c) PL excitation spectra of S-dots (black line, detected at 430 nm) and S-dots@PMDA (blue line, excited at 430 nm). (d) PL emission decay curves of S-dots (black line, excited at 360 nm), S-dots@PMDA (blue line, excited at 370 nm), and S-dots@BEU (cyan line, excited at 360 nm) detected at the peak maximum. (e) PL emission spectra of S-dots@BEU excited at different wavelengths. (f) PL emission (purple solid line, excited at 370 nm) and excitation (purple dotted line, detected at 425 nm) spectra of BEU and PL excitation spectra of S-dots (black dotted line, detected at 360 nm) and S-dots@BEU (cyan dotted line, detected at 360 nm).

on surface of S-dots, and new surface states, with an extended emission lifetime and lower excitation energy, were formed. Apparently, the newly formed surface states showed high PL intensities. In addition, PMDA was also linked with the –OH groups of S-dots through covalent bonds, accompanied by hydrogen bonds. S-dots were effectively isolated from quenching by oxygen or solvents, which also restricted the molecular motion and inhibited the nonradiative decay process.

Transferring S-dots into S-dots@BEU also resulted in an obvious increase in PL intensity and an extension of emission lifetime. This can also be attributed to the protection effect of BEU, which protected the emission center from quenching by oxygen or solvents, restricting the molecular motion and inhibiting the nonradiative decay process. However, the excitation-dependent emission properties of S-dots disappear (Fig. S7†), indicating the difference in the emission mechanism. To study the emission mechanism of S-dots@BEU, the photophysical properties of S-dots and BEU were studied and compared. As shown in Fig. 3f, BEU showed dual PL emission peaks at 345 and 425 nm and the first emission peak well-overlapped with the PL excitation spectrum of S-dots. Combining the closely connected structures of S-dots and BEU, energy transfer from BEU to S-dots may occur. This is confirmed by the disappearance of the first emission peak after processing BEU into S-dots and the well consistency of the emission peak of S-dots@BEU with the second emission peak of BEU (Fig. 3f). The composite materials of S-dots@BEU showed the integrated PL excitation behavior of S-dots and BEU without newly added or deleted absorption bands. This also confirmed the energy transfer from BEU to S-dots. Thus, the PL of S-dots@BEU was the integration of S-dots and BEU, and the

partial PL of BEU in the UV range transferred to S-dots. Thus, the emission of S-dots@BEU was attributed to the synthetic effects of the BEU matrix and energy transfer, which resulted in the increase of PL QY from 23% to 50% (Table S3†).

We also noted that transferring S-dots into S-dots @PMDA and S-dots@BEU resulted in the red shifting and blue shifting of the PL peak maximum. To gain more information on this phenomenon, temperature-dependent PL spectra were obtained. As shown in Fig. S8,† the PL intensity of three samples increased with the decrease of detection temperature, indicating the fluorescence nature of emission. There is no change in the peak shape and the shifting of the peak position in the temperature-dependent PL spectra of S-dots, while new peaks and shifting of the peak maximum were observed in the cases of S-dots @PMDA and S-dots@BEU. In the temperature-dependent PL spectra of S-dots@PMDA, decreasing the detection temperature resulted in a redshift of the peak maximum and a shoulder peak at around 500 nm was observed. This indicated the presence of multiple emission centres in the composites, which may be also related to the ester bonds between S-dots and PMDA. In contrast, a blue shift of the peak maximum was observed in the temperature-dependent PL spectra of S-dots@BEU, which originates from the molecular emission of BEU.

In addition, the composite of S-dots@PMDA and S-dots@BEU also showed excellent thermal stability. As shown in Fig. 4a and b and Fig. S9,† the fluorescence intensity of S-dots sharply decreased with the increase of detection temperature (from 25 to 140 °C) and the extension of heating time at 80 °C (0 to 10 h), which lost more than 40% of fluorescence intensity. In contrast, the fluorescence intensities of S-dots@PMDA and S-dots@BEU almost keep identical in the temperature range from 20 to 125 °C and during heating at 80 °C for 8 h (Fig. 4a and b, and Fig. S10†). These results demonstrated the excellent thermal stability of S-dots@PMDA and S-dots@BEU, attributed to the protection effects of PMDA and BEU. The hydrophobic chemical groups on PMDA and BEU played important roles in the improvement of thermal stability, which provided a protection layer on S-dots for the reaction with other external stimulations. In addition, the composites formed a dense matrix to inhibit the molecular motions of surface ligands, which was also helpful in improving thermal stability.

Utilizing the outstanding photophysical properties and the high thermal stability of these composite materials, their applications in fabricating LED devices were demonstrated. The powder of S-dots@PMDA showed a relatively wide blue emission from 400 to 550 nm at the excitation wavelength from 300 to 400 nm. To produce white light, yellow emissive phosphors were used to combine with S-dots. $(Sr,Ba)_3SiO_5$:Eu showed a yellow emission from 500 to 700 nm at the excitation wavelength from 300 to 500 nm. This confirmed the possibility to produce white light using a UV-emissive LED as the excitation light. Then LED devices with blue, yellow, and white emissions were developed by using S-dots@PMDA, $(Sr,Ba)_3SiO_5$:Eu, and their mixture as color conversion layers, respectively. The photographs of these devices are shown in Fig. 4d and the emission spectra of the operating devices are presented in Fig. 4e and f. Through modulating the ratio between S-dots@PMDA and $(Sr,Ba)_3SiO_5$:Eu, the CIE chromaticity coordinates of these devices tuned from blue (0.26, 0.25) to yellow (0.36, 0.36) through white. LED devices with a CIE chromaticity coordinate of (0.33, 0.32), a CCT of 5624 K and a high CRI of 91 were obtained. The optical stability of white LED devices was examined by studying their CIE chromaticity coordinates, CRIs, and CCTs in a rather wide range of operating working currents (from 20 to 250 mA). As shown in Table S4,† a slight variation of CIE chromaticity coordinates from (0.3089, 0.3287) to (0.3376, 0.3597) was observed, which was almost identical to that of pure white emission (0.33, 0.33). In addition, no obvious change in the CRI was also observed (from 89.1 to 84.4), which demonstrated their great potential for applications in lighting and display.

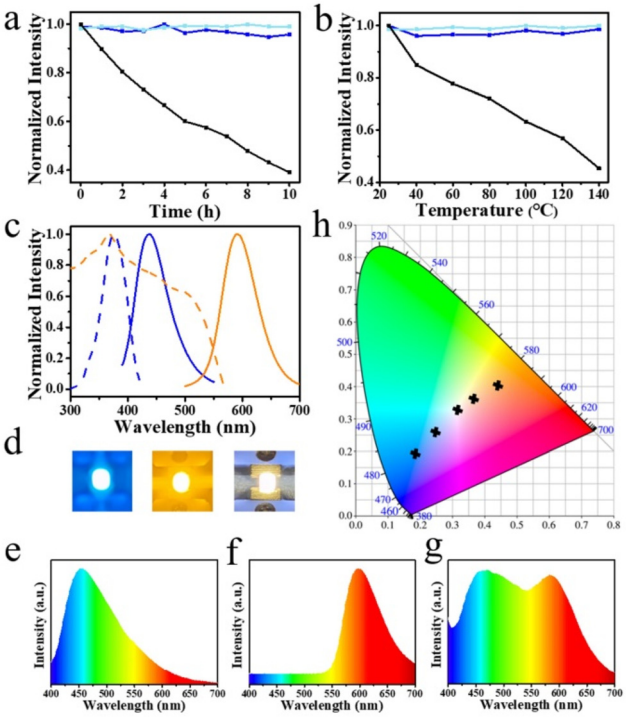

Fig. 4 Evolution of PL intensities at the peak maximum of S-dots (black line), S-dots@PMDA (blue line), and S-dots@BEU (cyan line) as a function of heating time (a) and heating temperature (b). (c) PL emission (solid line) and excitation (dotted line) of S-dots (blue colored) and (Sr, $Ba)_3SiO_5$:Eu (yellow colored). (d) Photographs of LED devices with blue, yellow and white emissions fabricated using S-dots@PMDA, $(Sr,Ba)_3SiO_5$: Eu, and their mixture as color conversion layers. (e–g) Emission spectra of blue, yellow, and white LED devices. (h) CIE color coordinates of LED devices fabricated using different ratios of S-dots@PMDA and (Sr, $Ba)_3SiO_5$:Eu as color conversion layers.

Experimental

Materials

Sublimed sulfur (99.5%), polyethylene glycol (M_n = 400) and pyromellitic dianhydride (99%) were obtained from Aladdin.

Hydrogen peroxide (30%) was obtained from Tianjin Damao Chemical Reagent Factory. Sodium hydroxide (99%) and benzoyleneurea (98%) were obtained from Innochem. Silicone OE-6551 A and OE-6551B parts were obtained from Dow Corning.

Characterization

An F-7000 spectrometer (Hitachi, Japan) was used to record the PL spectra. Time-resolved PL decay curves were obtained using an FLS980 spectrometer (Edinburgh Instruments) under excitation with a 375 nm laser diode, the decay curves were fitted based on a two-exponential fitting, and an average lifetime was calculated by summing the fitted time and percentage of the component. The absolute PL QY was determined on a Horiba Fluoromax + spectrofluorometer equipped with an integrating sphere. The surface morphologies of S-dots, S-dots@BEU and S-dots@PMDA were recorded using a JEOL-2100Plus transmission electron microscope (JEOL, JAPAN). UV–visible spectra were recorded on a Shimadzu UV3600 in reflectance mode using full reflection accessories with barium sulphate as the reference. Fourier transform infrared (FTIR) spectra were recorded on a Nicolet IS10 FTIR spectrometer (Thermo, USA). X-ray electron spectroscopy (XPS) spectra were recorded using a Thermo Scientific Escalab 250Xi+. Parameters of LEDs, including the Commission Internationale de l'Eclairage (CIE) color coordinates, color rendering index (CRI), and correlated color temperature (CCT), were on a high accuracy array rapid spectroradiometer (Haas-2000, Everfine Co., Ltd China) equipped with an integrating sphere.

Synthesis of S-dots@PMDA and S-dots@BEU

S-dots were prepared through a H_2O_2-assisted method. Typically, 1.4 g of sublimated sulfur, 3 mL of PEG-400 and 4 g of sodium hydroxide were added to 50 mL of water, which was heated at 90 °C for 72 h. Then, 2 mL of hydrogen peroxide was added to 10 mL of the above mixture. Under the irradiation of UV light, the mixture showed intensive blue emission, indicating the formation of S-dots. S-dots@PMDA was produced by injecting 0.08 g of PMDA into 10 mL of S-dots under stirring, followed by heating at 100 °C for 12 hours until forming a solid sample powder. S-dots@BEU was prepared by adding 0.005 g BEU into 10 mL of S-dots under stirring, followed by the same synthesis processes.

Fabrication of LEDs

Blue-emissive S-dots@PMDA (0.05 g) or orange-emissive (Sr, Ba)$_3$SiO$_5$:Eu (0.05 g) powder were mixed with silicone resins OE-6551 A (0.10 g) and OE-6551 B (0.20 g) to obtain monochrome blue LEDs or orange LEDs. White LEDs were assembled by mixing (Sr, Ba)$_3$SiO$_5$:Eu (0.0010 g) and S-dots@PMDA (0.6040 g) with OE-6551 A (0.1050 g) and OE-6551 B (0.2020 g). Part of the mixture was coated on the center of 365–370 nm GaN LED chips and transferred to an electric thermostatic blast oven for curing at 50 °C for 1 h.

Conclusions

In summary, surface modification and an assembly strategy were proposed to produce highly luminescent and thermally stable composites of S-dots@PMDA and S-dots@BEU. Assisted by the introduction of PMDA and BEU, the PL QY was improved to higher than 50%. In addition, the thermal stability of S-dots was also significantly improved. The structural and photophysical characterization results suggested that the introduction of PMDA eliminated the surface states of S-dots by forming covalent bonds. BEU resulted in the assembly of S-dots, which also allowed the energy transfer from BEU to S-dots. These outstanding photophysical features allowed us to develop LED devices by using the composites of S-dots as color-converting layers. Our synthetic strategy shows great potential for fabricating high-quality phosphors, which also provided a new idea for exploring the applications of S-dots in photoelectric devices.

Conflicts of interest

There are no conflicts to declare.

Acknowledgements

This work was financially supported by the National Natural Science Foundation of China (22175052), the Science Fund for Creative Research Groups of the Nature Science Foundation of Hebei Province (B2021201038), Central Government Guided Local Science and Technology Development Fund (Hebei), and the Research Innovation Team of College of Chemistry and Environmental Science of Hebei University (hxkytd-py2101).

References

1 A. Pal, F. Arshad and M. P. Sk, *Adv. Colloid Interface Sci.*, 2020, **285**, 102274.
2 Z. Wang, C. Zhang, H. Wang, Y. Xiong, X. Yang, Y. E. Shi and A. L. Rogach, *Angew. Chem., Int. Ed.*, 2020, **59**, 9997–10002.
3 W. Lu, Z. Wei, W. Guo, C. Yan, Z. Ding, C. Wang, G. Huang and V. M. Rotello, *Small*, 2023, **19**, 2301095.
4 R. Priyadarshi, A. Khan, P. Ezati, S. K. Tammina, S. Priyadarshi, T. Bhattacharya, J. T. Kim and J.-W. Rhim, *Environ. Chem. Lett.*, 2023, **21**, 1673–1699.
5 Y. E. Shi, P. Zhang, D. Yang and Z. Wang, *Chem. Commun.*, 2020, **56**, 10982–10988.
6 H. Ruan and L. Zhou, *Front. Bioeng. Biotechnol.*, 2022, **10**, 909727.
7 H. Jin, Y. Sun, Z. Sun, M. Yang and R. Gui, *Coord. Chem. Rev.*, 2021, **438**, 213913.
8 Y. Sheng, Z. Huang, Q. Zhong, H. Deng, M. Lai, Y. Yang, W. Chen, X. Xia and H. Peng, *Nanoscale*, 2021, **13**, 2519–2526.

9 K. Ning, Y. Sun, J. Liu, Y. Fu, K. Ye, J. Liang and Y. Wu, *Molecules*, 2022, **27**, 2822.
10 S. Mandal, B. Kommula and S. Bhattacharyya, *ACS Sustainable Chem. Eng.*, 2023, **11**, 14921–14931.
11 Y. Kumar, R. Kumar, P. Raizada, A. A. Parwaz Khan, V.-H. Nguyen, S. Y. Kim, Q. V. Le, R. Selvasembian, A. Singh, S. Gautam, C. C. Nguyen and P. Singh, *Chemosphere*, 2022, **305**, 135477.
12 C. Wang, Z. Wei, C. Pan, Z. Pan, X. Wang, J. Liu, H. Wang, G. Huang, M. Wang and L. Mao, *Sens. Actuators, B*, 2021, **344**, 130326.
13 L. Liu, Y. Zhang, R. Yuan and H. Wang, *Anal. Chem.*, 2020, **92**, 15112–15119.
14 T. Han, J. Yang, Y. Wang, Y. Cao, Y. Wang, H.-Y. Chen and J.-J. Zhu, *Electrochim. Acta*, 2021, **381**, 138281.
15 L. Shen, H. Wang, S. Liu, Z. Bai, S. Zhang, X. Zhang and C. Zhang, *J. Am. Chem. Soc.*, 2018, **140**, 7878–7884.
16 J. Ji and J. H. Choi, *Nanoscale*, 2022, **14**, 10648–10689.
17 Y. Sang, Q. Deng, F. Cao, Z. Liu, Y. You, H. Liu, J. Ren and X. Qu, *ACS Nano*, 2021, **15**, 19298–19309.
18 H. Wang, Z. Wang, Y. Xiong, S. V. Kershaw, T. Li, Y. Wang, Y. Zhai and A. L. Rogach, *Angew. Chem., Int. Ed.*, 2019, **58**, 7040–7044.
19 Y. Song, J. Tan, G. Wang, P. Gao, J. Lei and L. Zhou, *Chem. Sci.*, 2019, **11**, 772–777.
20 S. Liu, H. Wang, A. Feng, J. Chang, C. Zhang, Y.-E. Shi, Y. Zhai, V. Biju and Z. Wang, *Nanoscale Adv.*, 2021, **3**, 4271–4275.
21 C. Zhang, P. Zhang, X. Ji, H. Wang, H. Kuang, W. Cao, M. Pan, Y.-E. Shi and Z. Wang, *Chem. Commun.*, 2019, **55**, 13004–13007.
22 Z. Hu, H. Dai, X. Wei, D. Su, C. Wei, Y. Chen, F. Xie, W. Zhang, R. Guo and S. Qu, *RSC Adv.*, 2020, **10**, 17266–17269.
23 L. Xiao, Q. Du, Y. Huang, L. Wang, S. Cheng, Z. Wang, T. N. Wong, E. K. L. Yeow and H. Sun, *ACS Appl. Nano Mater.*, 2019, **2**, 6622–6628.
24 P. Gao, Z. Huang, J. Tan, G. Lv and L. Zhou, *ACS Sustainable Chem. Eng.*, 2022, **10**, 4634–4641.
25 B. Zheng, J. Fan, B. Chen, X. Qin, J. Wang, F. Wang, R. Deng and X. Liu, *Chem. Rev.*, 2022, **122**, 5519–5603.
26 M. Yu, M. H. Saeed, S. Zhang, H. Wei, Y. Gao, C. Zou, L. Zhang and H. Yang, *Adv. Funct. Mater.*, 2021, **32**, 2109472.
27 A. S. Pannu, S. Sen, X. Wang, R. Jones, K. Ostrikov and P. Sonar, *Nanoscale*, 2023, **15**, 2659–2666.
28 R. Priyadarshi, P. Ezati and J.-W. Rhim, *Environ. Chem. Lett.*, 2022, **20**, 3993–4008.
29 J. Guo, A. Feng, Y. E. Shi and Z. Wang, *Chem. – Eur. J.*, 2022, **28**, 202201990.
30 X. Yan, Y. Zhao, G. Du, Q. Guo, H. Chen, Q. He, Q. Zhao, H. Ye, J. Wang, Y. Yuan and T. Yue, *Chem. Eng. J.*, 2022, **433**, 133624.
31 X.-X. Jiang, P. Li, M.-Y. Zhao, R.-C. Chen, Z.-G. Wang, J.-X. Xie and Y.-K. Lv, *Anal. Chim. Acta*, 2022, **1221**, 340103.
32 Y. Zhang, J. Liu, X. Wu, W. Tao and Z. Li, *Anal. Chim. Acta*, 2020, **1131**, 68–79.
33 Z. Huang, J. Lei, H. Ruan, Y. Gong, G. Wang and L. Zhou, *Microchem. J.*, 2021, **164**, 106031.
34 J. Ren, L. Malfatti, L. Stagi, D. Carboni, R. Anedda, L. Calvillo and P. Innocenzi, *Chem. Mater.*, 2022, **34**, 8456–8468.
35 F. Arshad, M. P. Sk, S. K. Maurya and H. R. Siddique, *ACS Appl. Nano Mater.*, 2021, **4**, 3339–3344.
36 K. Nie, X. Wang, J. Qiu, Y. Wang, Q. Yang, J. Xu, X. Yu, H. Li, X. Huang and L. Chen, *ACS Energy Lett.*, 2020, **5**, 826–832.
37 S. Deng, J. Long, X. Dai, G. Wang and L. Zhou, *ACS Appl. Nano Mater.*, 2023, **6**, 1817–1827.
38 N. S. A. Manan, L. Aldous, Y. Alias, P. Murray, L. J. Yellowlees, M. C. Lagunas and C. Hardacre, *J. Phys. Chem. B*, 2011, **115**, 13873–13879.
39 C. Yi, W. Li, S. Shi, K. He, P. Ma, M. Chen and C. Yang, *Sol. Energy*, 2020, **195**, 340–354.
40 X. Wang, Y. Zhao, Q. Hua, J. Lu, F. Tang, W. Sun, F. Luan, X. Zhuang and C. Tian, *Analyst*, 2022, **147**, 1716–1721.
41 S. Li, D. Chen, F. Zheng, H. Zhou, S. Jiang and Y. Wu, *Adv. Funct. Mater.*, 2014, **24**, 7133–7138.